Convective and moist vorticity vectors associated with tropical oceanic convection: A three-dimensional cloud-resolving model simulation

Shouting Gao,[1] Xiaofan Li,[2] Wei-Kuo Tao,[3] Chung-Lin Shie,[4] and Steve Lang[5]

Received 8 February 2006; revised 13 September 2006; accepted 20 September 2006; published 13 January 2007.

[1] The relationships between cloud hydrometeors and convective/moist vorticity vectors are investigated using hourly data from a three-dimensional, 5-day cloud-resolving model (CRM) simulation during the Tropical Rainfall Measuring Mission (TRMM) Kwajalein Experiment (KWAJEX). Vertical components of convective and moist vorticity vectors are highly correlated with cloud hydrometeors. The vertical components represent the interaction between horizontal vorticity and horizontal moist potential temperature/specific humidity gradient. The vertical components of convective and moist vorticity vectors can be used to study tropical oceanic convection in both two-dimensional and three-dimensional frameworks.

Citation: Gao, S., X. Li, W.-K. Tao, C.-L. Shie, and S. Lang (2007), Convective and moist vorticity vectors associated with tropical oceanic convection: A three-dimensional cloud-resolving model simulation, *J. Geophys. Res.*, *112*, D01105, doi:10.1029/2006JD007179.

1. Introduction

[2] Clouds play an important role in regulating tropical climate. Although cloud formation and development are directly determined by cloud microphysical processes, the dynamic and thermodynamic processes determine cloud microphysical processes and play an indirect role in the evolution of convective systems. To understand important physical mechanisms that are responsible for convective development, physical parameters closely associated with convection are introduced so that physical laws can be applied to establish the framework for studying convection. Potential vorticity is one of such important physical quantities. Since introduced by *Ertel* [1942], dry and moist potential vorticity (PV) (PV = $\frac{\vec{\xi}\cdot\nabla\theta}{\rho}$, where $\vec{\xi}$ is the absolute vorticity, θ the potential temperature in dry air and equivalent potential temperature in moist air, ρ the air density, and ∇ the three-dimensional gradient operator) has enhanced the understanding of the dominant physical processes responsible for convection formation and growth for several decades [e.g., *Bennetts and Hoskins*, 1979; *Emanuel*, 1979; *Danielsen and Hipskind*, 1980; *Thorpe*, 1985; *Hoskins and Berrisford*, 1988; *Xu*, 1992; *Montgomery and Farrell*, 1993; *Cao and Cho*, 1995; *Cho and Cao*, 1998; *Gao et al.*, 2002] because of its conservation for frictionless moist adiabatic processes. The potential vorticity is not conserved when the diabatic heating occurs during the development of convection. The potential vorticity cannot be applied to the analysis of two-dimensional (2-D) model simulated data in the tropics since it could be zero for a 2-D equatorial circulation.

[3] To understand how the interaction between the circulation and clouds helps the growth of tropical convection, *Gao et al.* [2004] introduced a convective vorticity vector (CVV = $\frac{\vec{\xi}\times\nabla\theta_e}{\rho}$, where θ_e is equivalent potential temperature in moist air) to analyze tropical convection using results from 2-D cloud-resolving model (CRM) simulations. They showed that the vertical component of the CVV is closely associated with tropical convection and that its tendency is determined by the interaction between the vorticity and the zonal gradient of cloud heating. Since the moisture gradient is much more important than the temperature gradient in equivalent potential temperature gradient in the tropical environment, *Gao et al.* [2005] defined a moist vorticity vector (MVV = $\frac{\vec{\xi}\times\nabla q_v}{\rho}$, where q_v is specific humidity) for studying 2-D tropical convection and found that the vertical component of MVV and cloud hydrometeors are highly correlated and that its tendency is mainly determined by the interaction between the vorticity and the zonal gradient of condensational/depositional heating. The findings by *Gao et al.* [2004, 2005] were mainly based on 2-D data, then a question may be raised is how good the relationship between the three-dimensional (3-D) vorticity vectors (CVV and MVV) and convection could be.

[4] Since the horizontal rotational circulation is much stronger than secondary vertical circulation, PV mainly represents the covariance between vertical vorticity and vertical potential temperature gradient. Vertical components

[1]Laboratory of Cloud-Precipitation Physics and Severe Storms, Institute of Atmospheric Physics, Chinese Academy of Sciences, Beijing, China.
[2]Joint Center for Satellite Data Assimilation and Center for Satellite Applications and Research, National Environmental Satellite, Data, and Information Service, NOAA, Camp Springs, Maryland, USA.
[3]Laboratory for Atmospheres, NASA Goddard Space Flight Center, Greenbelt, Maryland, USA.
[4]Goddard Earth Sciences and Technology Center, University of Maryland Baltimore County, Baltimore, Maryland, USA.
[5]Science Systems and Applications Inc., Lanham, Maryland, USA.

Copyright 2007 by the American Geophysical Union.
0148-0227/07/2006JD007179

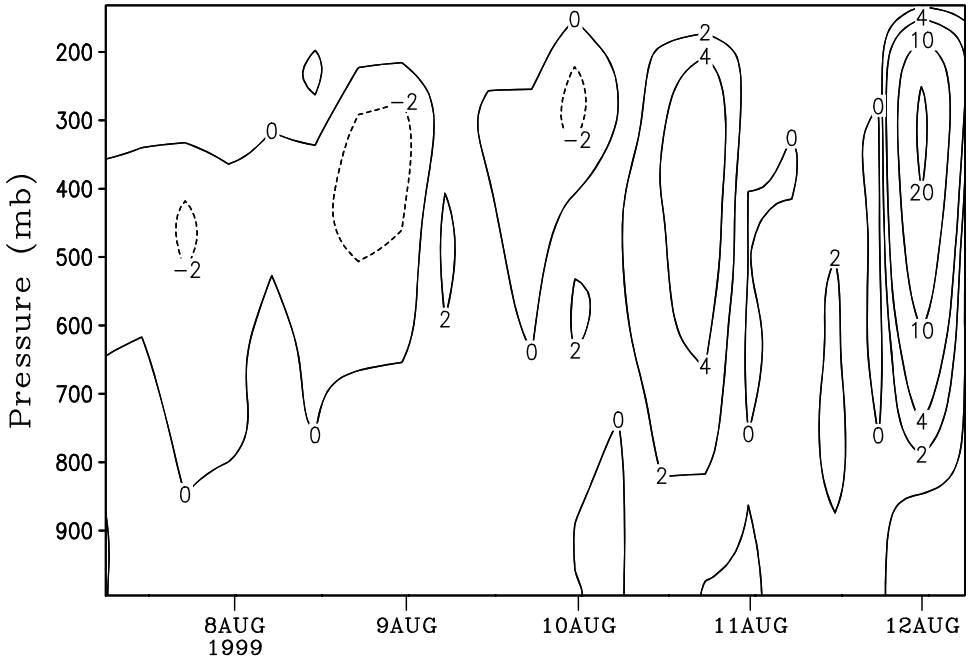

Figure 1. Temporal and vertical distribution of the vertical velocity during KWAJEX in the 5-day period. Unit is cm s^{-1}.

of CVV and MVV mainly denote interactions between horizontal vorticity and horizontal potential temperature/specific humidity gradient [*Gao et al.*, 2004, 2005]. The question is which quantity has better correlation with clouds.

[5] In this study, the data from a 3-D cloud-resolving simulation during the Tropical Rainfall Measuring Mission (TRMM) Kwajalein Experiment (KWAJEX) [e.g., *Yuter et al.*, 2005] are used to analyze CVV, MVV, and their relations to tropical oceanic convection as well as PV. The model and experiment are briefly described in the next section. Section 3 discusses CVV and PV, and section 4 presents results of MVV and MV. The summary is given in section 5.

2. Model and Experiment

[6] The model used in this study is the 3-D version of the Goddard Cumulus Ensemble (GCE) model. The GCE model was originally developed by *Soong and Ogura* [1980], *Soong and Tao* [1980], *Tao and Soong* [1986], and *Tao and Simpson* [1993]. The equations that govern cloud-scale motion (wind) are anelastic by filtering out sound waves. The subgrid-scale turbulence used in the GCE model is based on work by *Klemp and Wilhelmson* [1978]. In their approach, one prognostic equation is solved for subgrid kinetic energy, which is then used to specify the eddy coefficients. The effect of condensation on the generation of subgrid-scale kinetic energy is also incorporated in the model (see *Soong and Ogura* [1980] for details). The model also includes interactive solar [*Chou et al.*, 1998] and thermal infrared [*Chou et al.*, 1991; *Chou and Suarez*, 1994] radiation parameterization schemes. The model includes five prognostic equations for mixing ratios of cloud water, raindrop, cloud ice, snow, and graupel. The cloud microphysical parameterization schemes used in the model basically followed *Rutledge and Hobbs* [1983, 1984], *Lin et al.* [1983], and *Tao et al.* [1989, 2003].

[7] All scalar variables use forward time differencing and a positive definite advection scheme with a nonoscillatory option [*Smolarkiewicz and Grabowski*, 1990]. The dynamic variables use a second-order accurate advection scheme and a leapfrog time integration (kinetic energy semiconserving method). Details of the GCE model description are given by *Tao and Simpson* [1993] and *Tao et al.* [2003].

[8] Cyclic lateral boundaries are used. At the top of the model, a free-slip condition is used for horizontal winds, temperature, and specific humidity, and zero vertical velocity is applied. The horizontal domain is 512×512 km^2 with a horizontal grid resolution of 2 km. For the present study, a stretched vertical coordinate with 41 levels is used. The model has finer resolution (about 80 m) in the boundary layer and coarser resolution (about 1000 m) in the upper levels. The time step is 10 s. Surface fluxes from the ocean and cloud-radiation interactive processes are explicitly included. The observed sea surface temperature (SST) was used for latent and sensible heat flux calculations.

[9] The model is forced by zonally uniform vertical velocity, zonal wind, and thermal and moisture advection based on 6-hourly KWAJEX observations [*Shie et al.*, 2003]. Kwajalein Experiment field campaign was conducted from 23 July to 15 September 1999. Kwajalein island is located at 8.44°N, 167.43°E and has the area of 15 km^2, which is the largest island in Kwajalein Atoll (2200 km^2). From July to September, Kwajalein island is located around the northern edge of the western Pacific Intertropical Convergence Zone (ITCZ). Monthly rainfall increases from north to south around this region. *Shie et al.* [2003] conducted 3-D simulations and compared them with radar observations during three active periods in KWAJEX.

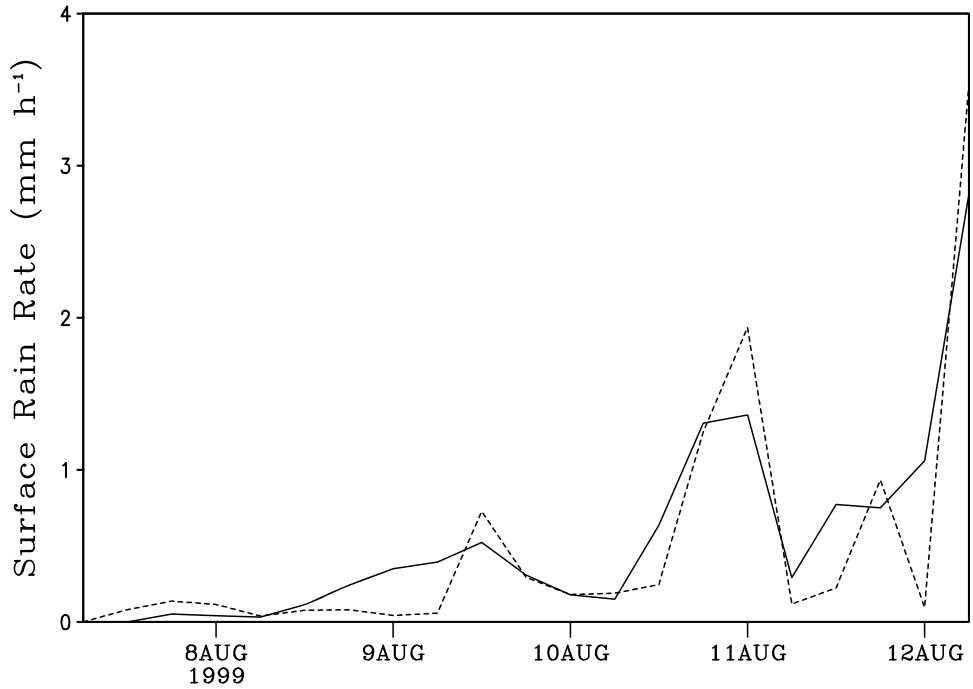

Figure 2. Time series of simulated (solid) and observed (dashed) domain-mean surface rain rates. Unit is mm h^{-1}.

The simulation and observation show reasonable agreement in rainfall, apparent heat and moisture sources from 7 to 12 August 1999. Thus their hourly zonal-mean simulation data from 0600 LST 7 August 1990 to 0600 LST 12 August 1999 (a total of 5 days) are analyzed in this study.

[10] Figure 1 shows the time evolution and vertical distribution of vertical velocity, which is imposed during 5-day integration. The weak upward motions appear from 8 to 9 August 1999, and they strengthen gradually. They reach their maximum of larger than 20 cm s^{-1} around 350 mbar at midnight of 11 August 1999.

[11] Figure 2 displays the time series of simulated and observed domain-mean surface rain rates. Both are highly correlated with a linear correlation coefficient of 0.92. The root-mean-squared differences between the simulated and observed surface rain rates are 0.36 mm h^{-1}, which are

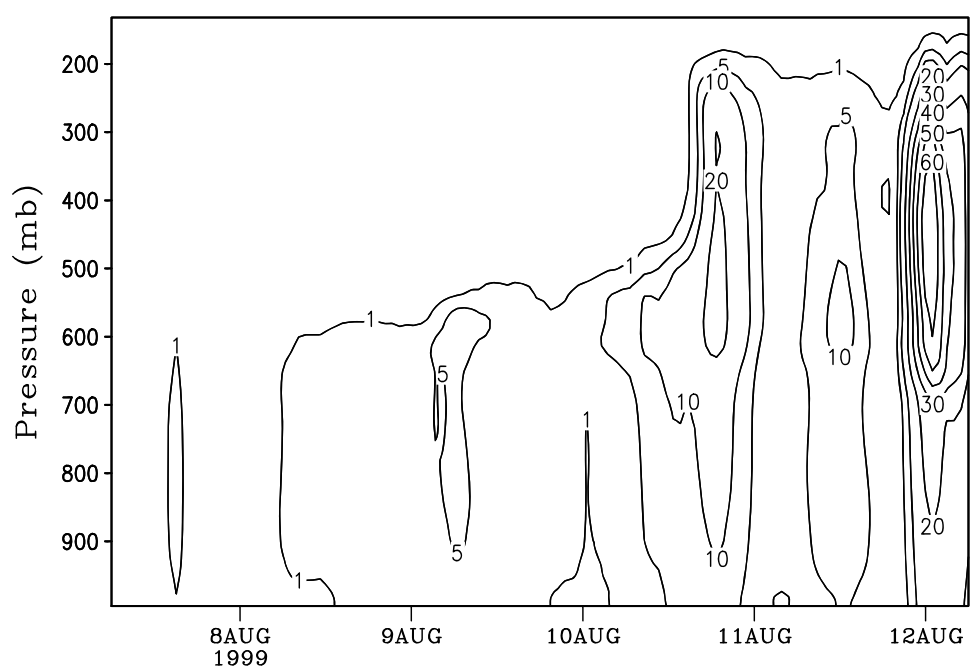

Figure 3. Temporal and vertical distribution of the sum of mixing ratios of cloud hydrometeors simulated during KWAJEX in the 5-day period. Unit is 10^{-2} g kg^{-1}.

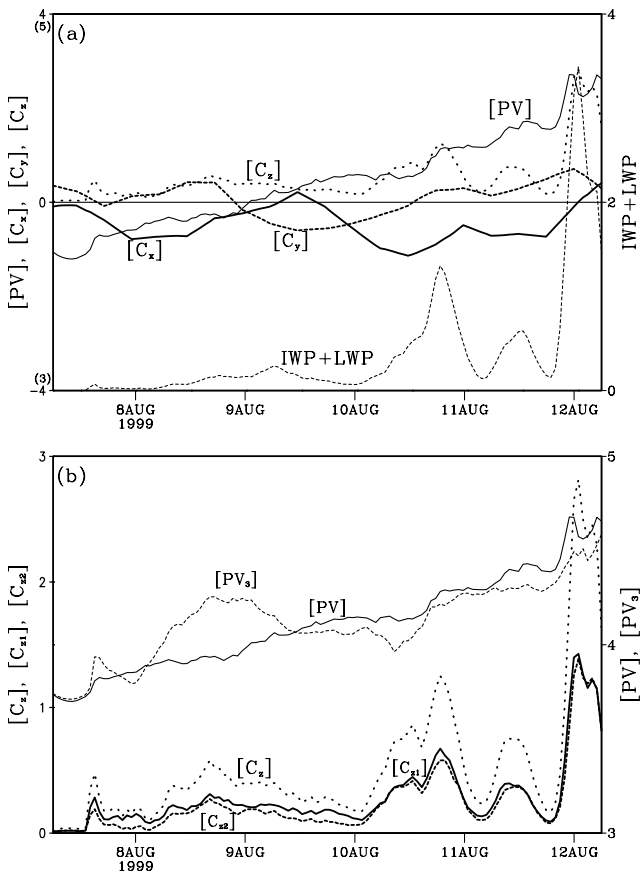

Figure 4. Time series of (a) IWP + LWP, [PV], $[C_x]$, $[C_y]$, and $[C_z]$ and (b) $[C_z]$, $[C_{z1}]$, $[C_{z2}]$, [PV], and $[PV_3]$. Units are mm for IWP + LWP; 10^{-3} K s^{-1} for [PV], $[PV_3]$, $[C_z]$, $[C_{z1}]$, and $[C_{z2}]$; and 10^{-1} K s^{-1} for $[C_x]$ and $[C_y]$. The plotting scales in Figure 4a are 3 to 5 $\times$ 10^{-3} K s^{-1} for [PV], -4 to 4 $\times$ 10^{-3} K s^{-1} for $[C_z]$, and -4 to 4 $\times$ 10^{-1} K s^{-1} for $[C_x]$ and $[C_y]$.

smaller than the standard derivations of the simulated (0.65 mm h^{-1}) and observed (0.84 mm h^{-1}) surface rain rates. The time-mean simulated surface rain rate (0.57 mm h^{-1}) is also similar to the time-mean observed surface rain rate (0.52 mm h^{-1}). This suggests that the simulation agrees well with the observation.

[12] Figure 3 shows the time evolution and vertical distribution of the sum of mixing ratios of cloud hydrometeors. The simulated clouds appear after 1200 LST 7 August 1999, and they strengthen gradually. They reach their maximum of larger than 0.6 g kg^{-1} around 450 mbar at midnight of 11 August 1999. The time evolution and vertical distribution of simulated clouds are similar to those of imposed vertical velocity, indicating the convective responses to imposed large-scale forcing.

3. Convective Vorticity Vector

[13] The 3-D CVV can be expressed by

$$\mathrm{CVV} = \frac{\vec{\xi} \times \nabla\theta_e}{\overline{\rho}} = C_x\vec{i} + C_y\vec{j} + C_z\vec{k}, \qquad (1)$$

where $C_x = \zeta_y\frac{\partial\theta_e}{\partial z} - \zeta_z\frac{\partial\theta_e}{\partial y}$, $C_y = \zeta_z\frac{\partial\theta_e}{\partial x} - \zeta_x\frac{\partial\theta_e}{\partial z}$, $C_z = \zeta_x\frac{\partial\theta_e}{\partial y} - \zeta_y\frac{\partial\theta_e}{\partial x}$; $\zeta_x = \frac{\partial w}{\partial y} - \frac{\partial v}{\partial z}$, $\zeta_y = \frac{\partial u}{\partial z} - \frac{\partial w}{\partial x}$, $\zeta_z = \frac{\partial v}{\partial x} - \frac{\partial u}{\partial y} + f$; u, v, w are zonal, meridional, and vertical components of wind; f is the Coriolis parameter.

[14] To compare CVV with PV, the PV is calculated. The PV can be expressed by

$$\mathrm{PV} = \frac{\vec{\xi} \cdot \nabla\theta_e}{\overline{\rho}} = PV_1 + PV_2 + PV_3, \qquad (2)$$

where $PV_1 = \zeta_x\frac{\partial\theta_e}{\partial x}$, $PV_2 = \zeta_y\frac{\partial\theta_e}{\partial y}$, $PV_3 = \zeta_z\frac{\partial\theta_e}{\partial z}$.

[15] Figure 4a shows the time series of IWP + LWP (the sum of ice and liquid water paths, that is, the sum of mass-integrated mixing ratios of cloud hydrometeors), $[C_x]$, $[C_y]$, and $[C_z]$ ([] is a mass integration). [PV] is included in Figure 4a for comparison with CVV. $[C_z]$ closely follows evolution of IWP + LWP whereas $[C_x]$ and $[C_y]$ do not. The linear correlation coefficient between $[C_z]$ and IWP + LWP is 0.97 whereas those between $[C_x]$ and IWP + LWP, and $[C_y]$ and IWP + LWP are 0.29 and 0.48, respectively. A Student's t-test on the significance of the correlation coefficients is further conducted using 118 degrees of freedom and a critical correlation coefficient at the 1% significance level is 0.24. Thus these relations are statically significant. The variances between IWP + LWP and $[C_z]$, IWP + LWP and $[C_x]$, and IWP + LWP and $[C_y]$ (that are calculated by the squares of the correlation coefficients) are 0.94, 0.08, 0.23, respectively. Thus the linear relation between IWP + LWP and $[C_z]$ is most robust. [PV] basically follows the evolution of cloud hydrometeors with the linear correlation coefficient of 0.73, which also exceeds the 1% significance level. Its variance is 0.53. From equation (2), [PV] is determined by three components. $[PV_3]$ have the similar magnitude to [PV] (Figure 4b) whereas two other components (not shown) are about one order of magnitudes smaller than $[PV_3]$. Thus [PV] is determined by the covariance between vertical component of vorticity (horizontal rotational circulations) and vertical gradient of moist potential gradient (stability parameter). Note that although the magnitude of $[PV_1]$ is small, the correlation coefficient between $[PV_1]$ and IWP + LWP is 0.54, which is slightly smaller than that between $[PV_3]$ and IWP + LWP (0.62). Since PV is a scalar, the role of horizontal component of vorticity in convective development cannot be analyzed.

[16] $[C_z]$ is determined by the covariance between horizontal components of vorticity (the secondary circulation in horizontal-vertical framework that is directly associated with the dynamic aspect of convection and is described by the zonal and meridional components of relative vorticity) and horizontal gradients of moist potential temperature (that is directly associated with the thermodynamic aspect of the convection). The secondary circulation is directly associated with vertical motion, which is a direct cloud producer. This explains why vertical component of CVV is highly correlated with cloud hydrometeors. The strong relationship between CVV and cloud hydrometeors implies that CVV can be a good physical vector for studying tropical convection. PV is associated with horizontal rotational circulation.

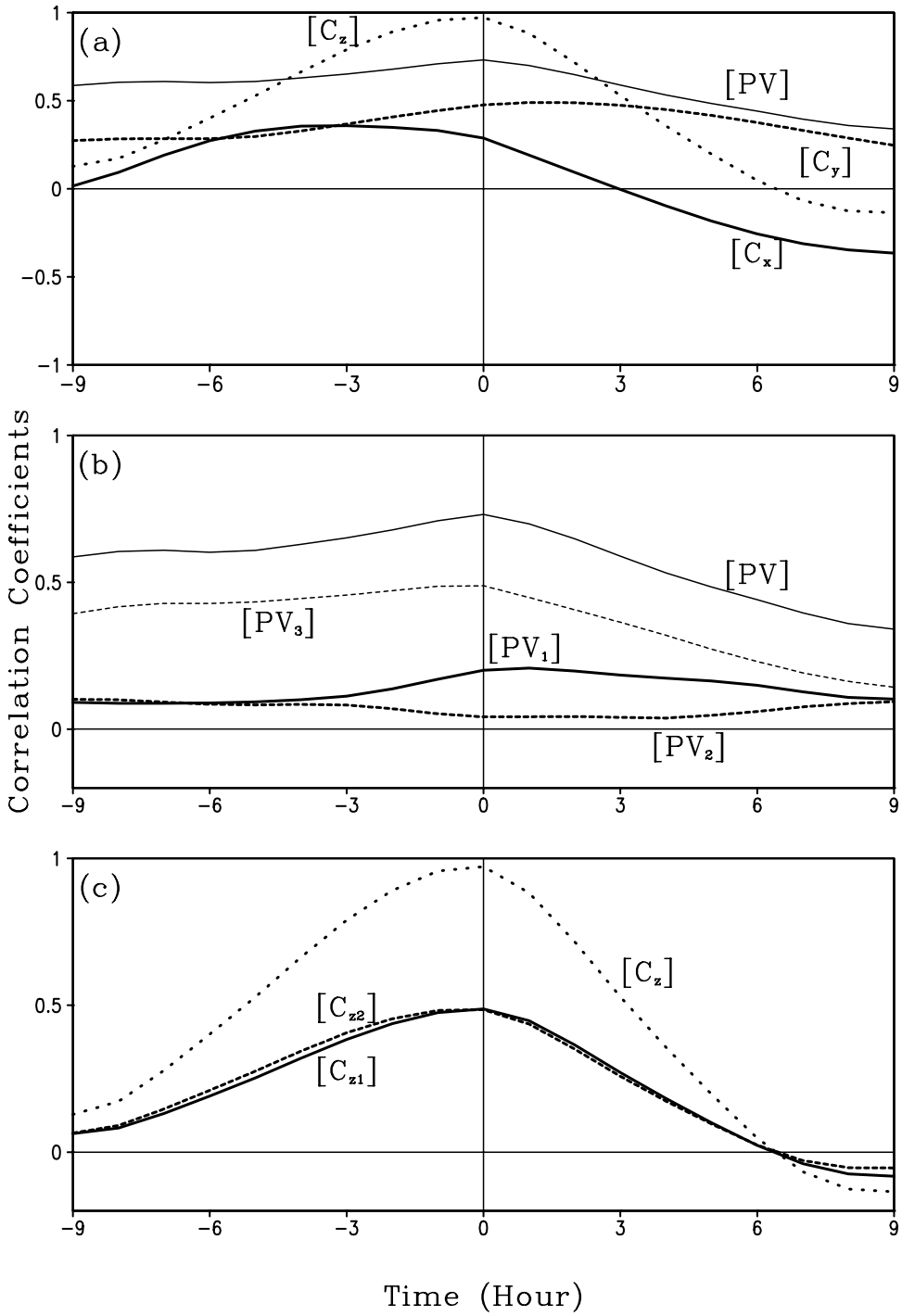

Figure 5. (a) Lag correlation coefficients between IWP + LWP and [PV], between IWP + LWP and [C_x], between IWP + LWP and [C_y], and between IWP + LWP and [C_z]; (b) lag correlation coefficients between IWP + LWP and [PV] and weighted lag correlation coefficients between IWP + LWP and [PV_1], between IWP + LWP and [PV_2], and between IWP + LWP and [PV_3]; and (c) lag correlation coefficients between IWP + LWP and [C_z] and weighted lag correlation coefficients between IWP + LWP and [C_{z1}] and between IWP + LWP and [C_{z2}].

Strong cyclonic circulation may not have a strong upward motion. This explains why the correlation between PV and cloud hydrometeors is weaker than that between CVV and cloud hydrometeors. The comparison between the PV and CVV shows that the vector analysis can be used to study the roles of horizontal and vertical components of vorticity in convective development separately.

[17] Figure 5a shows lag correlation coefficients between IWP + LWP and CVV and between IWP + LWP and PV. A positive (negative) lag hour denotes that maximum CVV or PV leads (lags) maximum IWP + LWP. [C_z] and [PV] are in phase with cloud hydrometeors. The in-phase relationship indicates that the vertical component of CVV can represent convection and a framework can be built from dynamic and

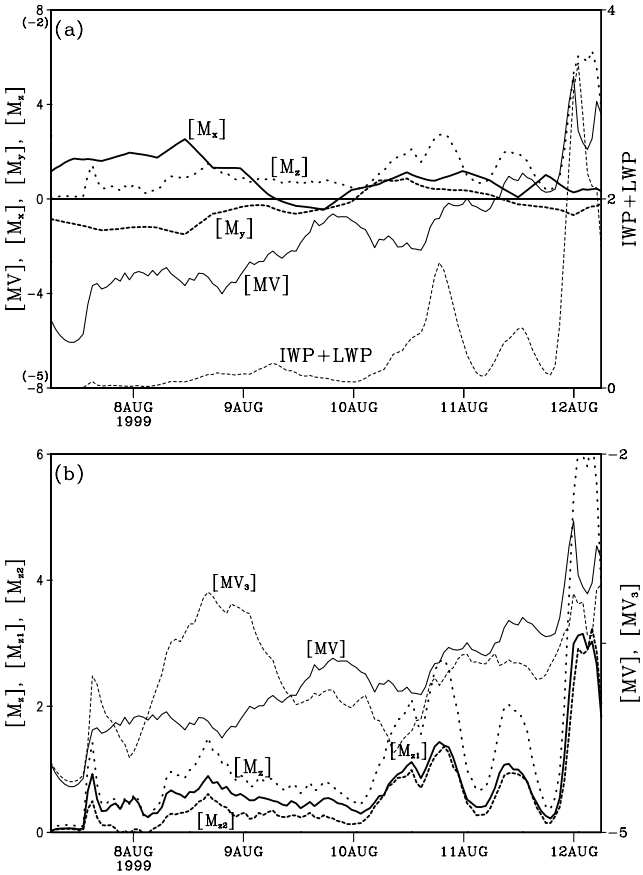

Figure 6. Time series of (a) IWP + LWP, [MV], [M_x], [M_y], and [M_z] and (b) [M_z], [M_{z1}], [M_{z2}], [MV], and [MV_3]. Units are mm for IWP + LWP; 10^{-7} s^{-1} for [MV], [MV_3], [M_z], [M_{z1}], and [M_{z2}]; and 10^{-5} s^{-1} for [M_x] and [M_y]. The plotting scales in Figure 6a are -5 to -2×10^{-7} s^{-1} for [MV], -8 to 8×10^{-7} s^{-1} for [M_z], and -8 to 8×10^{-5} s^{-1} for [M_x] and [M_y].

thermodynamic relations to study the physical processes that are responsible for the evolution of convection. [C_y] leads IWP + LWP by 1–2 hours. This suggests that meridional component of CVV can be served as a precursor for the occurrence of convection, which has a potential for the prediction of convection. [C_x] lags IWP + LWP by 3–4 hours. This may implies that convection feedbacks the dynamics and thermodynamics associated with clouds. To examine the contribution of [PV_1], [PV_2], and [PV_3] to the correlation between IWP + LWP and [PV], the weighted linear correlation coefficients between IWP + LWP and components of [PV] are calculated.

[18] For a scalar $F = \sum_{i=1}^{N} F_i$, its correlation coefficient with a scalar G can be expanded into

$$C_{G,F} = \sum_{i=1}^{N} \frac{\sigma_{F_i}}{\sigma_F} C_{G,F_i}, \tag{3}$$

where σ is a standard deviation; $\frac{\sigma_{F_i}}{\sigma_F} C_{G,F_i}$ is a weighted linear correlation coefficient between G and F_i; C_{G,F_i} is a linear correlation coefficient between G and F_i.

[19] Figure 5b shows lag correlation coefficients between IWP + LWP and components of [PV]. The lag correlation coefficient between IWP + LWP and [PV] is mainly determined by the weighted lag correlation coefficient between IWP + LWP and [PV_3], although one third of the lag correlation coefficient is contributed to by the weighted lag correlation coefficients between IWP + LWP and [PV_1] and between IWP + LWP and [PV_2].

[20] [C_z] can be broken down into [C_{z1}] and [C_{z2}], where $C_{z1} = \zeta_x \frac{\partial \theta_e}{\partial y}$, and $C_{z2} = -\zeta_y \frac{\partial \theta_e}{\partial x}$. Only [$C_{z2}$] appears in the 2-D framework. *Gao et al.* [2004] in their 2-D study of CVV during TOGA COARE showed the high linear correlation coefficient between [C_{z2}] and IWP + LWP. Figure 4b shows that [C_{z1}] and [C_{z2}] has similar evolution in both amplitudes and phases. To examine the contribution of [C_{z1}] and [C_{z2}] to the lag correlation between IWP + LWP and [C_z], the weighted lag correlation coefficients between IWP + LWP and [C_{z1}]/[C_{z2}] are calculated. The two correlation coefficients at lag hour 0 show same values, which indicate that [C_{z1}] and [C_{z2}] equally contribute to the correlation coefficient between cloud hydrometeors and vertical component of CVV. Thus the vertical component of CVV can be a controlling parameter for studying tropical oceanic convection, regardless of the dimension of data (2-D or 3-D).

4. Moist Vorticity Vector

[21] The 3-D MVV can be expressed by

$$\mathrm{MVV} = \frac{\vec{\xi} \times \nabla q_v}{\overline{\rho}} = M_x \vec{i} + M_y \vec{j} + M_z \vec{k}, \tag{4}$$

where $M_x = \zeta_y \frac{\partial q_v}{\partial z} - \zeta_z \frac{\partial q_v}{\partial y}$, $M_y = \zeta_z \frac{\partial q_v}{\partial x} - \zeta_x \frac{\partial q_v}{\partial z}$, $M_z = \zeta_x \frac{\partial q_v}{\partial y} - \zeta_y \frac{\partial q_v}{\partial x}$. Since moisture gradient is much more important than temperature gradient in the tropics, it determines the variation of moist potential temperature gradient [e.g., *Gao et al.*, 2005]. Thus $\frac{\vec{\xi} \cdot \nabla q_v}{\overline{\rho}}$ is defined as the moist vorticity (MV). To compare MVV with MV, the MV is calculated. The MV can be expressed by

$$\mathrm{MV} = \frac{\vec{\xi} \cdot \nabla q_v}{\overline{\rho}} = MV_1 + MV_2 + MV_3, \tag{5}$$

where $MV_1 = \zeta_x \frac{\partial q_v}{\partial x}$, $MV_2 = \zeta_y \frac{\partial q_v}{\partial y}$, $MV_3 = \zeta_z \frac{\partial q_v}{\partial z}$.

[22] Figure 6a shows the time series of IWP + LWP, [M_x], [M_y], and [M_z]. [MV] is included in Figure 6a for comparison with MVV. Like CVV, vertical component of MVV intimately follows the variation of IWP + LWP with the correlation coefficient of 0.95. [MV] and IWP + LWP are also highly correlated with the coefficient of 0.75. [MV_3] have the similar magnitude to [MV] (Figure 6b) whereas two other components (not shown) are about one order of magnitudes smaller than [MV_3]. Unlike CVV, horizontal components of MVV ([M_x] and [M_y]) are loosely correlated with cloud hydrometeors for only -0.26 and 0.17, respectively, which are marginally statistically significant and not statistically significant (Figure 7a). The weighted lag cor-

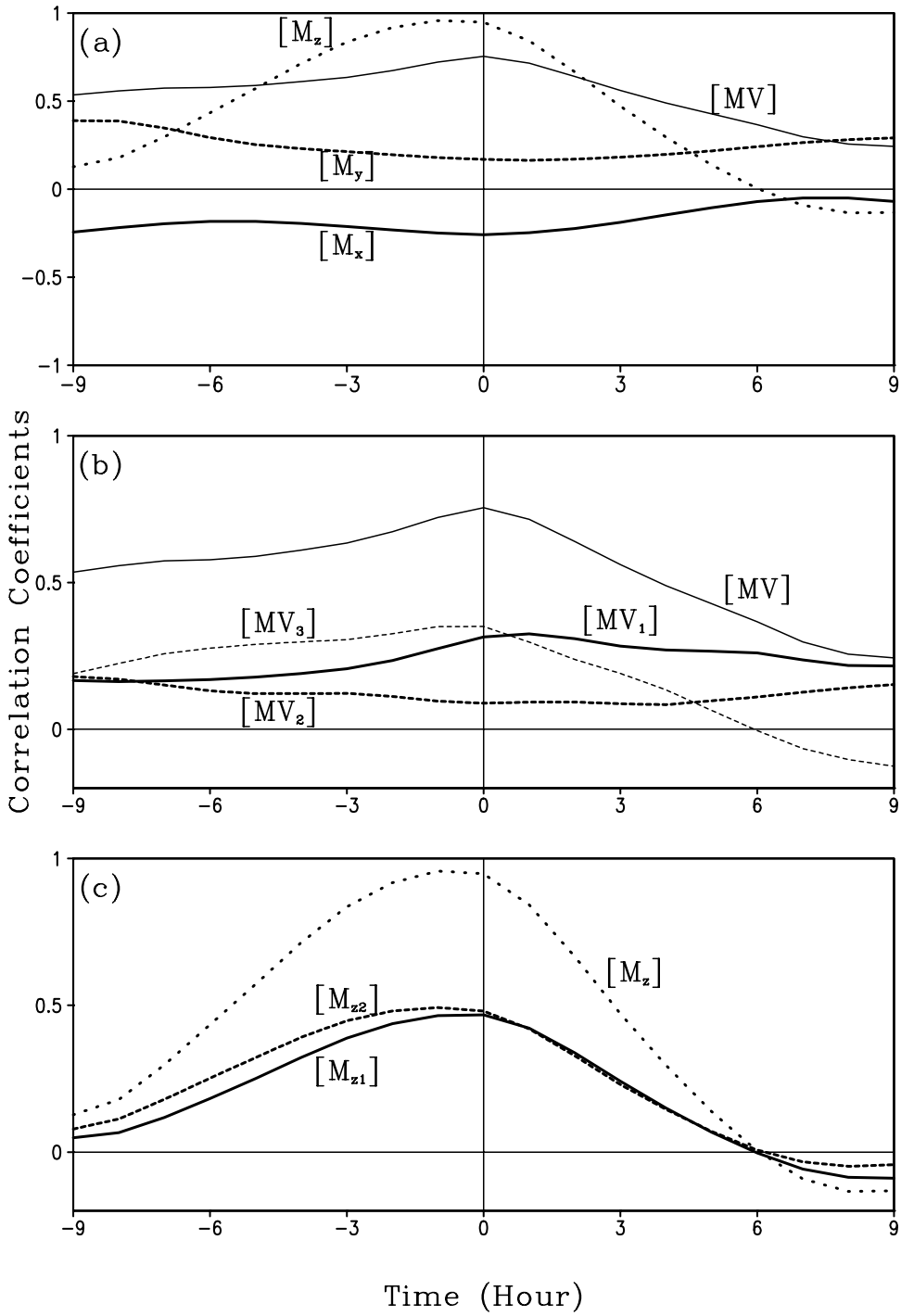

Figure 7. (a) Lag correlation coefficients between IWP + LWP and [MV], between IWP + LWP and [M_x], between IWP + LWP and [M_y], and between IWP + LWP and [M_z]; (b) lag correlation coefficients between IWP + LWP and [MV] and weighted lag correlation coefficients between IWP + LWP and [MV_1], between IWP + LWP and [MV_2], and between IWP + LWP and [MV_3]; and (c) lag correlation coefficients between IWP + LWP and [M_z] and weighted lag correlation coefficients between IWP + LWP and [M_{z1}] and between IWP + LWP and [M_{z2}].

relation coefficients between IWP + LWP and [MV_3] and between IWP + LWP and [MV_1] have important contribution to the lag correlation coefficient between IWP + LWP and [MV] (Figure 7b), although the magnitude of [MV_1] is much smaller than that of [MV_3]. The maximum correlation coefficient between IWP + LWP and [M_z] is 0.96 at lag hour −1, which is mainly contributed to by the lag correlation between IWP and LWP and [M_{z1}] (Figure 7c). This indicates that [M_z] lags IWP + LWP by 1 hour. [M_z] can be broken down into [M_{z1}] and [M_{z2}], where $M_{z1} = \zeta_x \frac{\partial q_v}{\partial y}$, and

$M_{z2} = -\zeta_y \frac{\partial q_v}{\partial x}$. Only [$M_{z2}$] appears in the 2-D framework. *Gao et al.* [2005] showed the high linear correlation coefficient between [M_{z2}] and IWP + LWP. [M_{z1}] is slightly larger than [M_{z2}] when the convection is moderate or strong (e.g., from 0000 LST 10 August 1999 to 0600 LST 12 August 1999), whereas [M_{z1}] is significantly larger when the convection is weak (e.g., from 1200 LST 7 August 1999 to 0000 LST 10 August 1999) (Figure 6b). Thus the vertical component of MVV can be a controlling parameter for studying tropical oceanic convection, in particular strong convection, regardless of the dimension of data (2-D or 3-D). The weighted lag correlation coefficient between IWP + LWP and [M_{z2}] is larger than that between IWP + LWP and [M_{z1}] at negative lag hour (Figure 7c), suggesting that it contributes to the vertical component of MVV lagging cloud hydrometeors by 1 hour.

5. Summary

[23] Convective and moist vorticity vectors and their relationships to cloud hydrometeors are investigated using data from a three-dimensional cloud-resolving simulation. The model is integrated for selected 5 days during KWAJEX. The linear correlation coefficients between cloud hydrometeors and vertical components of convective and moist vorticity vectors are significantly larger than those between cloud hydrometeors and corresponding horizontal (zonal and meridional) components. The linear correlation coefficients between cloud hydrometeors and vertical components of convective and moist vorticity vectors are larger than the correlation coefficient between cloud hydrometeors and moist potential vorticity, a classic physical parameter for studying convective activity. These indicate that the interaction between horizontal vorticity and horizontal moist potential temperature/specific humidity gradient is intimately associated with tropical oceanic convection. The vertical components of convective and moist vorticity vectors have two contributors: interactions between zonal vorticity and meridional moist potential temperature/specific humidity gradient (that vanishes in 2-D x-z framework), and meridional vorticity and zonal moist potential temperature/specific humidity gradient. Both have similar time evolutions and magnitudes, in particular, when convection is strong. Thus the vertical components of convective and moist vorticity vectors can be used to study evolution of tropical oceanic convection, regardless of dimension of simulation data.

[24] Different dynamic and thermodynamic characteristics between PV and CVV and between MV and MVV can be used to identify convective systems such as stratiform rainfall system associated with a strong horizontal rotational circulation and a weak upward motion, and heavy rainfall system associated with a strong upward motion. The comparison between PV and MV and between CVV and MVV can be used to study the roles of temperature gradients and water vapor gradients in frontal development in midlatitude and convective development in tropics. Since the analysis of CVV and MVV is limited to numerical data, further analysis should apply to observational data.

[25] **Acknowledgments.** S. Gao is supported by the National Natural Sciences Foundation of China 40433007, "Outstanding Oversea Scholars" project 2005-2-17 and National Key Basic Research and Development project of China 2004CB418301. W.-K. Tao, C.-L. Shie and S. Lang are supported by the NASA Headquarters Atmospheric Dynamics and Thermodynamics Program and the NASA Tropical Rainfall Measuring Mission (TRMM). The authors are grateful to R. Kakar at NASA headquarters for support. The authors also thank M. Zhang and his research group at the State University of New York, Stony Brook, for providing the observational data including the large-scale advective forcing in Kwajalein Atoll of the Republic of the Marshall Islands and two anonymous reviewers for their constructive comments that improved the manuscript significantly. Acknowledgment is also made to the NASA Goddard Space Flight Center for computer time used in this research.

References

Bennetts, D. A., and B. J. Hoskins (1979), Conditional symmetric instability–A possible explanation for frontal rainbands, *Q. J. R. Meteorol. Soc.*, *105*, 945–962.

Cao, Z., and H. Cho (1995), Generation of moist vorticity in extratropical cyclones, *J. Atmos. Sci.*, *52*, 3263–3281.

Cho, H., and Z. Cao (1998), Generation of moist vorticity in extratropical cyclones. Part II: Sensitivity to moisture distribution, *J. Atmos. Sci.*, *55*, 595–610.

Chou, M.-D., and M. J. Suarez (1994), An efficient thermal infrared radiation parameterization for use in general circulation model, *NASA Tech. Memo. 104606*, vol. 3, 85 pp., NASA Goddard Space Flight Center, Greenbelt, Md. (Available at http://dao.gsfc.nasa.gov/pubs/docs/Chou128).

Chou, M.-D., D. P. Kratz, and W. Ridgway (1991), Infrared radiation parameterization in numerical climate models, *J. Clim.*, *4*, 424–437.

Chou, M.-D., M. J. Suarez, C.-H. Ho, M. M.-H. Yan, and K.-T. Lee (1998), Parameterizations for cloud overlapping and shortwave single scattering properties for use in general circulation and cloud ensemble models, *J. Atmos. Sci.*, *55*, 201–214.

Danielsen, E. F., and R. S. Hipskind (1980), Stratospheric-tropospheric exchange at polar latitudes in summer, *J. Geophys. Res.*, *85*(C1), 393–400.

Emanuel, K. A. (1979), Inertial instability and mesoscale convective systems. Part I: Linear theory of inertial instability in rotating viscous fluids, *J. Atmos. Sci.*, *36*, 2425–2449.

Ertel, H. (1942), Ein neuer hydrodynamischer wirbelsatz, *Meteorol. Z. Braunschweigs*, *6*, 277–281.

Gao, S.-T., T. Lei, and Y.-S. Zhou (2002), Moist potential vorticity anomaly with heat and mass forcings in torrential rain system, *Chin. Phys. Lett.*, *19*, 878–880.

Gao, S., F. Ping, X. Li, and W.-K. Tao (2004), A convective vorticity vector associated with tropical convection: A 2D cloud-resolving modeling study, *J. Geophys. Res.*, *109*, D14106, doi:10.1029/2004JD004807.

Gao, S., X. Cui, Y. Zhou, X. Li, and W.-K. Tao (2005), A modeling study of moist and dynamic vorticity vectors associated with 2D tropical convection, *J. Geophys. Res.*, *110*, D17104, doi:10.1029/2004JD005675.

Hoskins, B. J., and P. Berrisford (1988), A potential vorticity perspective of the storm of 15–16 October 1987, *Weather*, *43*, 122–129.

Klemp, J. B., and R. B. Wilhelmson (1978), The simulation of three-dimensional convective storm dynamics, *J. Atmos. Sci.*, *35*, 1070–1093.

Lin, Y.-L., R. D. Farley, and H. D. Orville (1983), Bulk parameterization of the snow field in a cloud model, *J. Clim. Appl. Meteorol.*, *22*, 1065–1092.

Montgomery, M. T., and B. F. Farrell (1993), Tropical cyclone formation, *J. Atmos. Sci.*, *50*, 285–310.

Rutledge, S. A., and P. V. Hobbs (1983), The mesoscale and microscale structure and organization of clouds and precipitation in midlatitude cyclones. Part VIII: A model for the "seeder-feeder" process in warm-frontal rainbands, *J. Atmos. Sci.*, *40*, 1185–1206.

Rutledge, S. A., and P. V. Hobbs (1984), The mesoscale and microscale structure and organization of clouds and precipitation in midlatitude cyclones. Part XII: A diagnostic modeling study of precipitation development in narrow cold-frontal rainbands, *J. Atmos. Sci.*, *41*, 2949–2972.

Shie, C.-L., W.-K. Tao, and J. Simpson (2003), Simulated KWAJEX convective systems using a 2D and 3D cloud resolving model and their comparisons with radar observations, in *Proceedings of the 31st Conference on Radar Meteorolology*, pp. 441–444, Am. Meteorol. Soc., Boston, Mass.

Smolarkiewicz, P. K., and W. W. Grabowski (1990), The multidimensional positive advection transport algorithm: Non-oscillatory option, *J. Comput. Phys.*, *86*, 355–375.

Soong, S. T., and Y. Ogura (1980), Response of tradewind cumuli to large-scale processes, *J. Atmos. Sci.*, *37*, 2035–2050.

Soong, S. T., and W.-K. Tao (1980), Response of deep tropical cumulus clouds to mesoscale processes, *J. Atmos. Sci.*, *37*, 2016–2034.

Tao, W.-K., and J. Simpson (1993), The Goddard Cumulus Ensemble Model. Part I: Model description, *Terr. Atmos. Oceanic Sci.*, *4*, 35–72.

Tao, W.-K., and S.-T. Soong (1986), A study of the response of deep tropical clouds to mesoscale processes: Three-dimensional numerical experiments, *J. Atmos. Sci.*, *43*, 2653–2676.

Tao, W.-K., J. Simpson, and M. McCumber (1989), An ice-water saturation adjustment, *Mon. Weather Rev.*, *117*, 231–235.

Tao, W.-K., C.-L. Shie, J. Simpson, S. Braun, R. H. Johnson, and P. E. Ciesielski (2003), Convective systems over the South China Sea: Cloud-resolving model simulations, *J. Atmos. Sci.*, *60*, 2929–2956.

Thorpe, A. J. (1985), Diagnosis of balanced vortex structure using potential vorticity, *J. Atmos. Sci.*, *42*, 397–406.

Xu, Q. (1992), Formation and evolution of frontal rainbands and geostrophic potential vorticity anomalies, *J. Atmos. Sci.*, *49*, 629–648.

Yuter, S. E., R. A. Houze Jr., E. A. Smith, T. T. Wilteit, and E. J. Zipser (2005), Physical characterization of tropical oceanic convection observed in KWAJEX, *J. Appl. Meteorol.*, *44*, 385–415.

S. Gao, Laboratory of Cloud-Precipitation Physics and Severe Storms, Institute of Atmospheric Physics, Chinese Academy of Sciences, Beijing 100029, China. (gst@lasg.iap.ac.cn)

S. Lang, Science Systems and Applications Inc., Lanham, MD 20706, USA.

X. Li, Joint Center for Satellite Data Assimilation and Center for Satellite Applications and Research, National Environmental Satellite, Data, and Information Service, NOAA, Camp Springs, MD 20746, USA.

C.-L. Shie, Goddard Earth Sciences and Technology Center, University of Maryland Baltimore County, Baltimore, MD 21250, USA.

W.-K. Tao, Laboratory for Atmospheres, NASA Goddard Space Flight Center, Greenbelt, MD 20771, USA.